

Applicability of ${}^9\text{Be}$ global optical potential to description of ${}^{8,10,11}\text{B}$ elastic scattering*

Yong-Li Xu(徐永丽)^{1,1)} Yin-Lu Han(韩银录)^{2,2)} Hai-Ying Liang(梁海英)² Zhen-Dong Wu(吴振东)²
 Hai-Rui Guo(郭海瑞)³ Chong-Hai Cai(蔡崇海)⁴

¹College of Physics and Electronic Science, Shanxi Datong University, Datong 037009, China

²Key Laboratory of Nuclear Data, China Institute of Atomic Energy, Beijing 102413, China

³Institute of Applied Physics and Computational Mathematics, Beijing 100094, China

⁴Department of Physics, Nankai University, Tianjin 300071, China

Abstract: We achieved a set of ${}^9\text{Be}$ global phenomenological optical model potentials by fitting a large experimental dataset of the elastic scattering observable for target mass numbers from 24 to 209. The obtained ${}^9\text{Be}$ global optical model potential was applied to predict elastic-scattering angular distributions and total reaction cross-sections of ${}^{8,10,11}\text{B}$ projectiles. The predictions are made by performing a detailed analysis comparing with the available experimental data. Furthermore, these elastic scattering observables are also predicted for some lighter targets outside of the given mass number range, and reasonable results are obtained. Possible physical explanations for the observed differences are also discussed.

Keywords: optical model potential, elastic-scattering angular distribution, total reaction cross section

DOI: 10.1088/1674-1137/44/3/034101

1 Introduction

In the last few years, reactions involving ${}^{8,10,11}\text{B}$ isotopes have increasingly been attracting intense experimental and theoretical attention. The optical model potential (OMP) plays an important role in the investigation of these reactions. Theoretical studies have already been performed on this subject using both phenomenological and microscopic approaches. In this study, the phenomenological OMP are discussed with the aim to describe elastic scattering. Since the global phenomenological OMP is achieved by fitting large quantities of experimental data in a certain range of energy and mass, the basic elastic scattering observables can be reliably predicted using it in the region where no experimental measurement data exist [1]. Thus far, the experimental data of elastic scattering involving ${}^{8,10,11}\text{B}$ projectiles are relatively scarce, because the radioactive beams are not produced at sufficiently high intensities [2]. Therefore, it is difficult to achieve reliable global OMP on the basis of existing experimental data.

In our previous work, the elastic scattering observ-

able for ${}^{8,10,11}\text{B}$ isotopes has been predicted using the global phenomenological OMP of the ${}^7\text{Li}$ projectile. Reasonable agreement is obtained between the predictions and corresponding experimental data for ${}^{8,10}\text{B}$. However, the global OMP of ${}^7\text{Li}$ cannot provide a good description for backward-angle area for ${}^{11}\text{B}$, and the radius parameter of the real part potential was adjusted to improve the fit for ${}^{11}\text{B}$ on the basis of ${}^7\text{Li}$ global OMP [3]. Recently, the global phenomenological OMP of ${}^9\text{Be}$ was achieved by simultaneously fitting the experimental data of elastic-scattering angular distributions and total reaction cross-sections below 200 MeV in the range of target mass from 24 to 209 [4]. Moreover, the stable weakly bound projectile ${}^9\text{Be}$ is adjacent to the ${}^{8,10,11}\text{B}$ isotopes. Within this context, we intend to apply the obtained global phenomenological OMPs of ${}^9\text{Be}$ to perform a systematic study involving the elastic scattering of ${}^{8,10,11}\text{B}$ isotopes impinging on different targets, which can further study the nuclear reaction and structure properties for ${}^{8,10,11}\text{B}$ projectiles.

This paper is constructed as follows. In Sec. 2, the phenomenological OMP formula and methods used in

Received 9 November 2019, Published online 6 January 2020

* Supported by the National Natural Science Foundation of China (11405099 and 11575291). This work is also a part of IAEA Coordinated Research Projects (CRPs) on Recommended Input Parameter Library (RIPL) for Fission Cross Section Calculations (20464)

1) E-mail: xuyongli776@126.com

2) E-mail: hanyl@ciae.ac.cn

©2020 Chinese Physical Society and the Institute of High Energy Physics of the Chinese Academy of Sciences and the Institute of Modern Physics of the Chinese Academy of Sciences and IOP Publishing Ltd

this work are described for the elastic scattering of $^{8,10,11}\text{B}$ projectiles. The elastic scattering observables describing the reactions induced by $^{8,10,11}\text{B}$ are predicted using the global OMP of ^9Be , which are further discussed by comparison with the existing experimental data. Finally, the main conclusions of this work are summarized in Sec. 3.

2 Optical model calculations and discussion

As previously outlined [4], the optical model potential of the Woods-Saxon type,

$$V(r, E) = V_R(E)f(r, R_R, a_R) + iW_V(E)f(r, R_V, a_V) + i(-4W_S(E)a_S)\frac{d}{dr}f(r, R_S, a_S), \quad (1)$$

and Coulomb potential of a uniform charged sphere with radius R_C were used in OM calculations. $V_R(E)$, $W_S(E)$, and $W_V(E)$ are the energy-dependent potential depths, and they are respectively expressed as

$$V_R(E) = V_0 + V_1E + V_2E^2, \quad (2)$$

$$W_S(E) = \max\{0, W_0 + W_1E\}, \quad (3)$$

$$W_V(E) = \max\{0, U_0 + U_1E\}. \quad (4)$$

The radial functions are given by

$$f(r, R_i, a_i) = 1 + \exp[(r - R_i)/a_i]^{-1}, \quad (5)$$

$$R_i = r_iA^{\frac{1}{3}}, \quad i = R, S, V, C, \quad (6)$$

where A depicts the target mass number. r_R , r_S , r_V , and r_C are the radius parameters of real, surface, volume imaginary, and Coulomb potentials, respectively. a_R , a_S , and a_V are the corresponding diffuseness parameters. The radius parameters of the real potential is expressed by

$$r_R = r_{R_0} + r_{R_1}A^{\frac{1}{3}}. \quad (7)$$

We achieved a set of ^9Be global OMP parameters on the basis of experimental data of elastic-scattering angular distributions and total reaction cross-sections in the mass number range from 24 to 209 below 100 MeV [4]. The parameters of global OMP are listed in Table 1.

In what follows, we apply the obtained ^9Be global OMP to predict elastic scattering observables for $^{8,10,11}\text{B}$ projectiles and compared this with the available experimental data.

2.1 Elastic scattering of ^8B

The radioactive nucleus ^8B is a lighter nucleus far from the β -stability valley, which is widely discussed as a candidate for a first proton drip line nucleus with a proton halo [5]. The proton separation energy is only 137 keV. Thus far, there were various reports on ^8B in the literature studying its properties and the respective influences on different reaction mechanisms, because of the relevance of ^8B in astrophysics, nuclear structure, and re-

Table 1. Global phenomenological OMP parameters for ^9Be .

parameter	value	unit
V_0	268.0671	MeV
V_1	-0.180	
V_2	-0.0009	
W_0	52.149	MeV
W_1	-0.125	
U_0	2.965	MeV
U_1	0.286	
r_{R_0}	1.200	fm
r_{R_1}	0.0273	fm
r_S	1.200	fm
r_V	1.640	fm
r_C	1.556	fm
a_R	0.726	fm
a_S	0.843	fm
a_V	0.600	fm

action theories [6]. However, the elastic scattering data with this projectile remain scarce because of the extreme difficulty to obtain reasonably intense beams [7]. To date, the elastic-scattering angular distributions and the total reaction cross-sections of ^8B have been measured for ^{12}C , ^{27}Al , ^{28}Si , ^{58}Ni , and ^{208}Pb targets [6, 8-16]. These observables are predicted using obtained global OMP of ^9Be and compared with those predicted using global OMP of ^7Li [3]. Further, since ^8Li is the mirror nucleus of ^8B , they are also predicted using our global OMP of ^8Li [17]. These predictions are compared with existing experimental data.

Figure 1 presents the comparison of elastic-scattering angular distributions with the experimental data [6] for the $^8\text{B} + ^{27}\text{Al}$ system at incident energies of 15.3 MeV and 21.7 MeV. The figure shows that all of these global OMPs can reasonably predict the corresponding experimental data, and these predictions are relatively closed. The elastic-scattering angular distributions for the $^8\text{B} + ^{58}\text{Ni}$ system are predicted and compared with the experimental data [8] from 20.7 to 29.3 MeV, which is shown in Fig. 2. Although there is some divergence among these results predicted using the different global OMPs, all of them can reasonably generate the experimental data within the error range.

For the $^8\text{B} + ^{208}\text{Pb}$ system, elastic-scattering angular distributions are also measured at incident energies of 50.0, 170.3, and 178.0 MeV [9-11]. They are further predicted using different global OMPs. The results are in good agreement with these existing experimental data [10, 11] at 170.3 MeV and 178.0 MeV. As for the incident energy of 50.0 MeV, the global OMP of ^8Li can provide a more satisfactory description of the experiment-

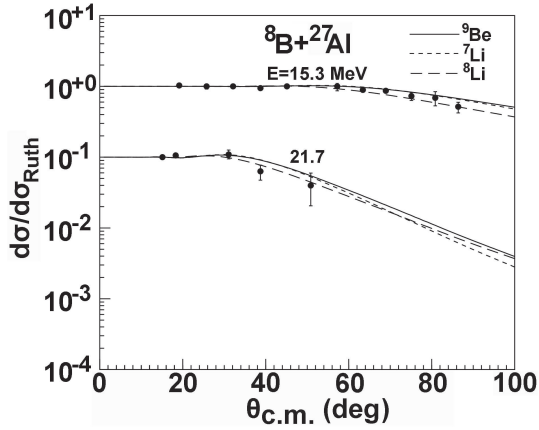


Fig. 1. Comparisons of ^8B elastic-scattering angular distributions calculated using ^9Be , ^7Li and ^8Li global OMPs with corresponding experimental data for ^{27}Al .

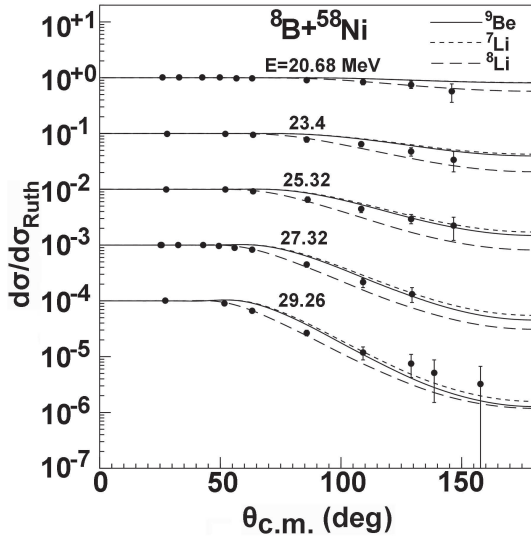


Fig. 2. Same as Fig. 1, but for ^{58}Ni .

al data [9] compared with the global OMPs of ^9Be and ^7Li at backward angles. These results are shown in Fig. 3.

Further, elastic-scattering angular distributions are also predicted using different global OMPs for the lighter target ^{12}C . Comparing with experimental data [12, 13], these predictions seem inaccurate, as there is some divergence at extreme values. The result is shown in Fig. 4. Since the reactions of the lighter targets ($A < 24$) induced by different weakly bound nuclei ^9Be , ^7Li , and ^8Li were not included in the process of adjusting the global OMP parameters, they should be studied using the local OMP.

To date, the total reaction cross-sections had been only measured for the $^8\text{B} + ^{28}\text{Si}$ system [14–16], and most of them are above 200 MeV. The comparison between the predictions and data from different experiments below 250 MeV are shown in Fig. 5, which exhibits some divergences between them.

From the above comparisons, the theoretical results

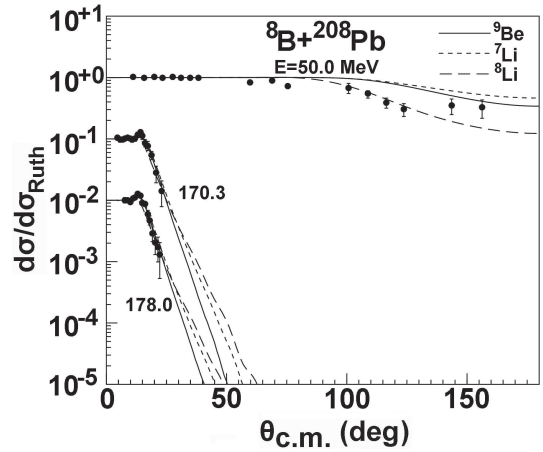


Fig. 3. Same as Fig. 1, but for ^{208}Pb .

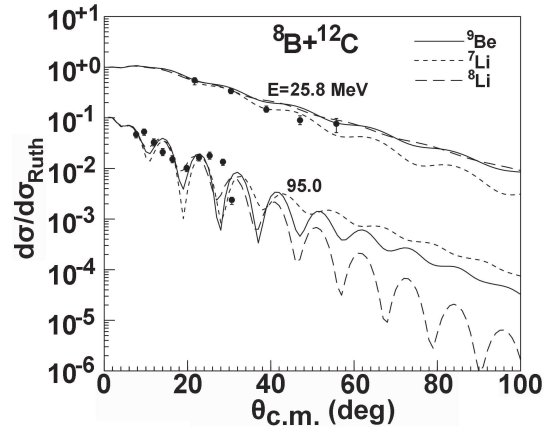


Fig. 4. Same as Fig. 1, but for ^{12}C .

predicted using the global OMPs of ^9Be and ^7Li can provide a reasonable description of the reactions induced ^8B within the allowed error range, although it seems that the predictions of global OMP ^8Li are more consistent with the few existing experimental data.

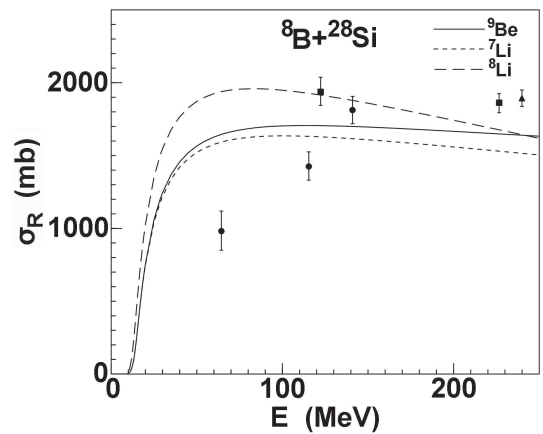


Fig. 5. Comparisons of ^8B total reaction cross-sections calculated using ^9Be , ^7Li and ^8Li global OMPs with corresponding experimental data for ^{28}Si .

2.2 Elastic scattering of ^{10}B

In the case of the ^{10}B projectile, the elastic-scattering angular distributions and total reaction cross-sections are predicted using the global OMPs of ^9Be and ^7Li .

Figures 6 and 7 present the comparisons of elastic-scattering angular distributions between theoretical predictions and experimental data [18] for ^{27}Al and $^{28,30}\text{Si}$ targets at the bombarding energies from 33.7 MeV to 50 MeV. Figure 6 shows slight oscillations in the angular distributions appearing in the angular range from 50° to 80° , while agreement between the predictions of ^9Be global OMP and experimental data is rather good.

For the target ^{58}Ni , the angular distributions are pre-

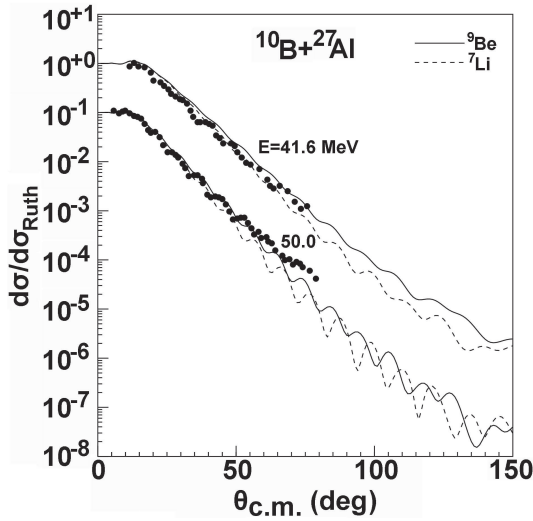


Fig. 6. Comparisons of ^{10}B elastic-scattering angular distributions calculated using ^9Be and ^7Li global OMPs with corresponding experimental data for ^{27}Al .

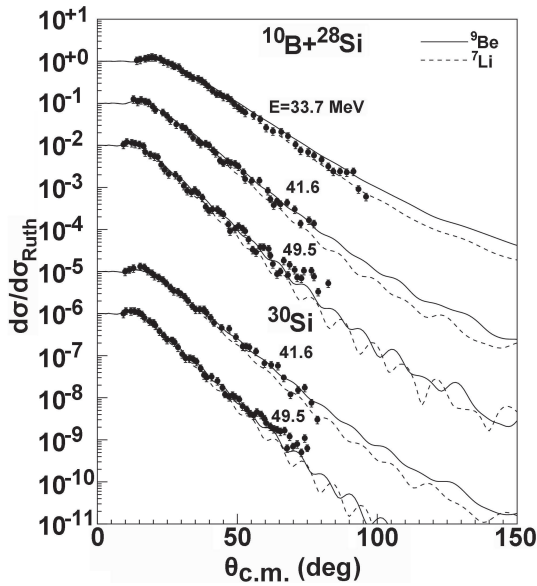


Fig. 7. Same as Fig. 6, but for $^{28,30}\text{Si}$.

dicted using global OMPs of ^9Be and ^7Li at incident energies from 19.0 MeV to 35.0 MeV. In comparison with the experimental data [19], the predictions provide a good description of these data, which is shown in Fig. 8. The elastic-scattering angular distributions for ^{10}B on ^{120}Sn were measured at the bombarding energies of 31.5, 33.5, 35.0, and 37.5 MeV [20]. Global OMPs of the ^9Be and ^7Li were used to describe the experimental data. The ^9Be global OMP provides a better description of experimental data. The result is displayed in Fig. 9.

Figure 10 presents the theoretical results of angular distributions along with experimental measurements [21–23] for different targets. The theoretical results predicted using global OMPs of ^9Be and ^7Li give a satisfactory description for ^{40}Ca and ^{208}Pb . There are some discrepancies between them for lighter targets ^{16}O and ^{20}Ne , while the results of ^9Be global OMP are more consistent with the corresponding measurements.

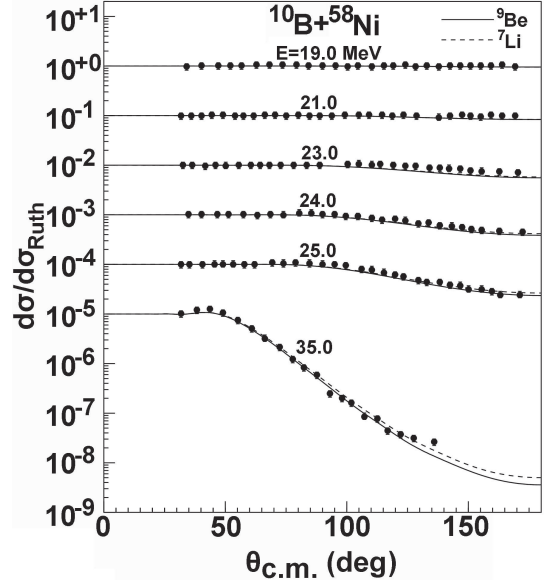


Fig. 8. Same as Fig. 6, but for ^{58}Ni .

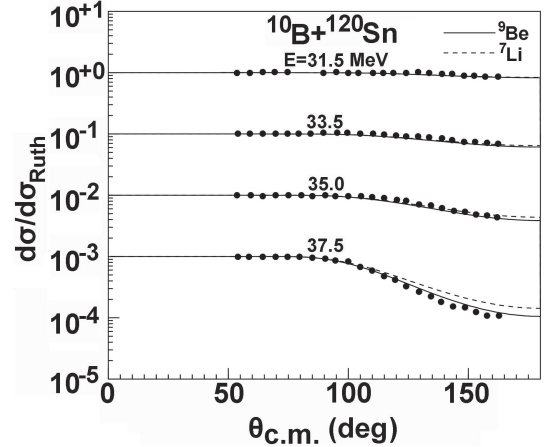


Fig. 9. Same as Fig. 6, but for ^{120}Sn .

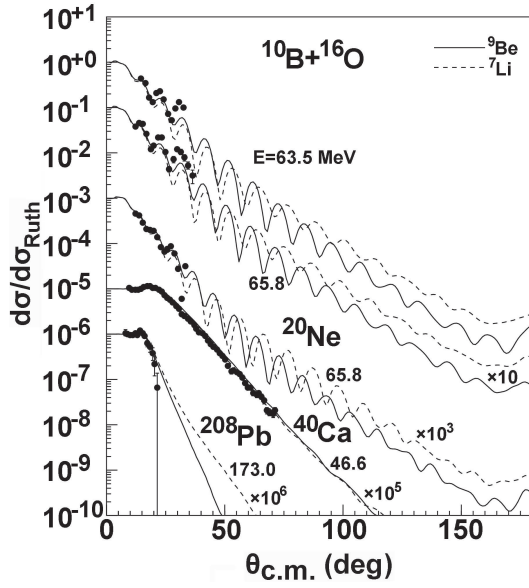


Fig. 10. Same as Fig. 6, but for ^{16}O , ^{20}Ne , ^{40}Ca , and ^{208}Pb .

For the other lighter targets, the elastic-scattering angular distributions are also measured by different experiments. These reactions are further predicted using different global OMPs. Figure 11 presents the comparisons between them for ^9Be . The discrepancy observed in Fig. 11 between theory and experiment [24, 25] indicates that the addition of coupled channels effects is needed in the backward-angle area for some lighter targets.

For the total reaction cross-sections of ^{10}B , there are only the experimental data for $^{\text{nat}}\text{Si}$. We compare the predicted results of total reaction cross-sections to the experimental data [16, 26, 27] for ^{28}Si . The result is shown in Fig. 12. The results of the ^9Be global OMP are completely in agreement with all of the experimental data within the error range. For ^{208}Pb , the data of total reaction cross-sections [23] was derived in terms of the optical model by analyzing the elastic scattering data at different incident energies. The predictions of the global OMP

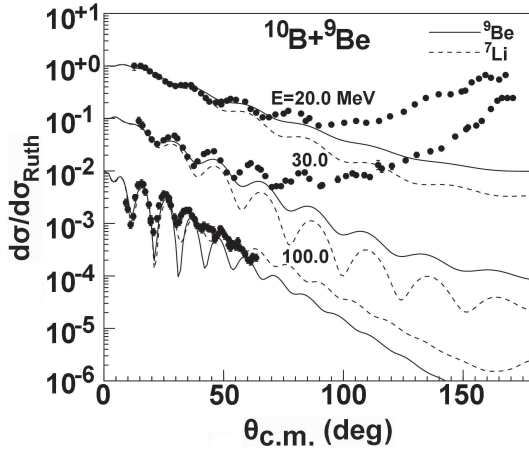


Fig. 11. Same as Fig. 6, but for ^9Be .

of ^9Be and ^7Li are also compared with the data, which is shown in Fig. 13. All of them are in good agreement.

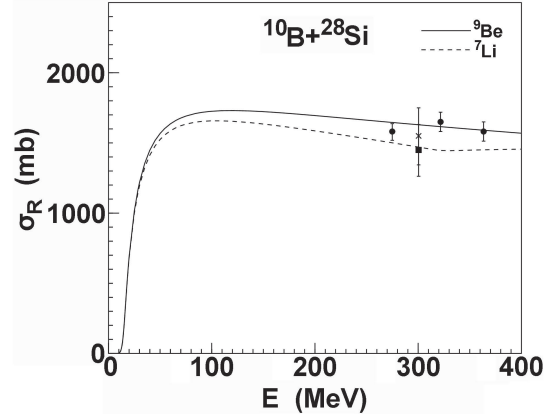


Fig. 12. Comparison of ^{10}B total reaction cross-sections calculated using ^9Be and ^7Li global OMPs with corresponding experimental data for ^{28}Si .

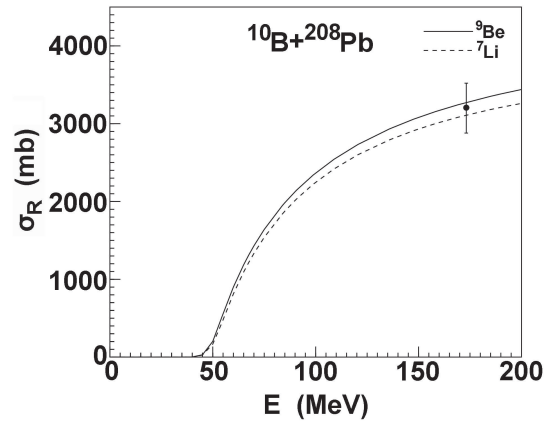


Fig. 13. Same as Fig. 12, but for ^{208}Pb .

2.3 Elastic scattering of ^{11}B

For the ^{11}B projectile, we obtained the global OMP [3] by adjusting the radius parameters of the real part potential on the basis of global OMP of ^7Li . Although the predictions gave a reasonable description of the ^{11}B elastic scattering for most of targets, the OMP cannot provide a satisfactory agreement with the experimental data in the backward-angle area for a few targets. In this section, the elastic scattering observables are predicted using the global OMPs of ^9Be and ^{11}B . The predictions are further compared with the existing experimental data.

Figure 14 presents the comparisons of elastic-scattering angular distributions between theoretical predictions and experimental data [18] for $^{28,30}\text{Si}$ targets at the bombarding energies from 33.7 MeV to 50 MeV. The fits are generally reasonable with no apparent systematic nor major discrepancy of the data. However, the results predicted using the global OMP of ^9Be are more consistent with the experimental data.

The elastic-scattering angular distributions for ^{58}Ni are measured at incident energies from 19.0 MeV to 35.0 MeV [28]. The comparison between the predictions and experimental data is shown in Fig. 15. The figure shows that the predictions using global OMPs of ^9Be and ^{11}B are almost consistent and in good agreement with the data, except for 35.0 MeV, where the prediction using the global OMP ^{11}B is more consistent with the experimental data. Moreover, the elastic angular distributions for ^{58}Ni are measured at the same incident angle with different incident energies [29]. Comparisons of the predictions of elastic-scattering angular distributions from the global OMP of ^9Be and ^{11}B show that all of them are identical and can reproduce the data, which is shown in Fig. 16.

For ^{40}Ca and ^{208}Pb , the elastic angular distributions are measured at incident energies of 51.5 MeV and 69.0 MeV [21, 30]. Figure 17 presents the comparisons between the predictions and experimental data. The predictions of ^9Be and ^{11}B are in good agreement with the experimental data. For ^{209}Bi , the angular distributions for elastic scattering calculated using the ^{11}B global OMP were larger than the experimental data [30, 31] at backward angles. Hence, the radius of the real part for the ^{11}B global phenomenological OMP was added by 0.15 to improve the fit with the data [3]. Figure 18 presents the theoretical results predicted using the global OMPs of ^9Be and ^{11}B together with the experimental data. From the figure, one can see that the calculations of ^9Be global OMP are in excellent agreement with the experimental data at all energies. Compared to those of the global OMP ^{11}B , the global OMP of ^9Be can give a better prediction for the

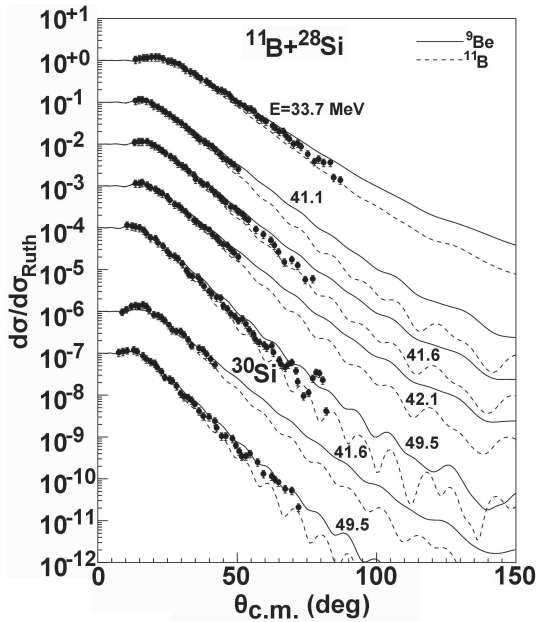


Fig. 14. Comparisons of ^{11}B elastic-scattering angular distributions calculated using ^9Be and ^{11}B global OMPs with corresponding experimental data for $^{28,30}\text{Si}$.

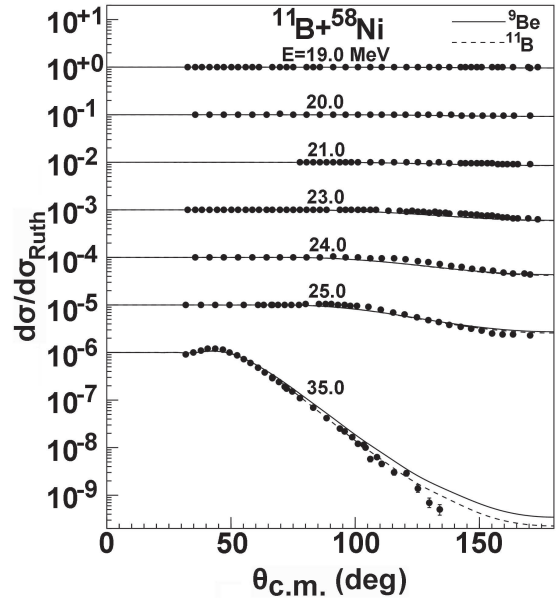


Fig. 15. Same as Fig. 14, but for ^{58}Ni .

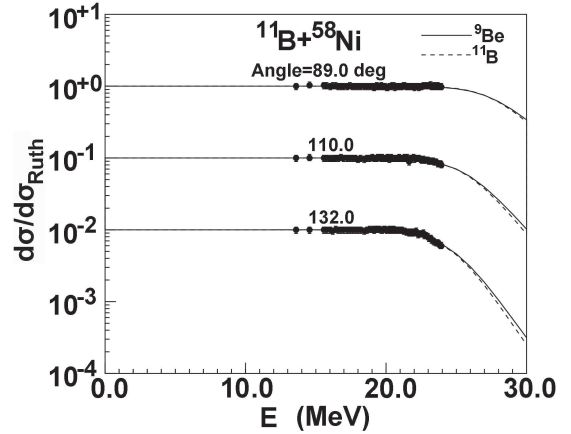


Fig. 16. Calculated elastic-scattering angular distributions in Rutherford ratio at same incident angles compared with experimental data for ^{58}Ni target.

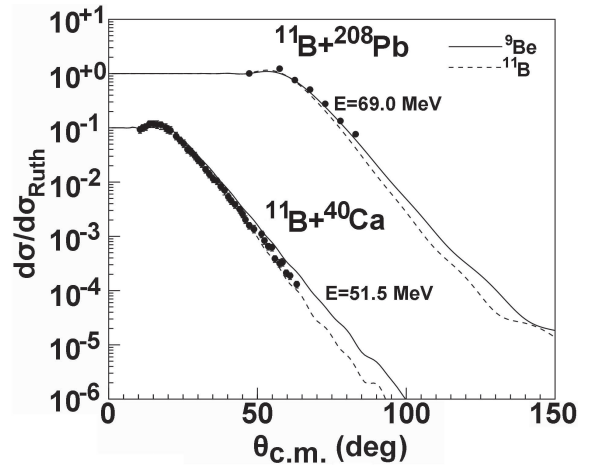


Fig. 17. Same as Fig. 14, but for ^{40}Ca and ^{208}Pb .

$^{11}\text{B} + ^{209}\text{Bi}$ reaction. One of the reasons may be that the ^{11}B global OMP was obtained by only adjusting the radius parameters of the real part potential on the basis of the global OMP of ^7Li [3], since the existing experimental data on elastic scattering is scarce for the reactions induced by the ^{11}B projectile. Moreover, this may be the influence of target shell effects for the doubly closed shell ^{208}Pb nucleus and one proton outside the closed shell ^{209}Bi nucleus. Meanwhile, the radius parameter of the real potential of the global OMP ^9Be was further defined by $r_{R_0} + r_{R_1} A^{\frac{1}{3}}$ as compared to r_{R_0} of the global OMP ^{11}B , which may compensate the influence of target shell effects.

Similarly, the elastic-scattering angular distributions for some lighter targets are predicted using the global OMPs of ^9Be and ^{11}B . Figure 19 presents the comparisons for $^{12,13}\text{C}$. The discrepancy observed in Fig. 19 between theory and experiment [32–34] shows that it possibly requires the addition of coupled channels effects in the backward-angle area for some lighter targets.

There are no measurements of the total reaction cross-sections for the reactions induced by ^{11}B . The existing data of total reaction cross-sections for ^{209}Bi were extracted from the experimental elastic scattering data [31]. The predictions of total reaction cross-sections are further compared with the data for ^{209}Bi , which is shown in Fig. 20. The predictions are in satisfactory agreement with the data extracted from the measured elastic-scattering angular distributions.

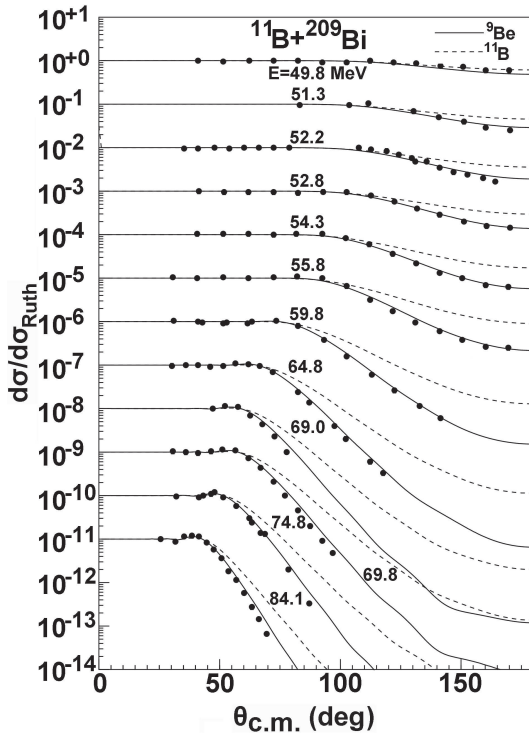


Fig. 18. Same as Fig. 14, but for ^{209}Bi .

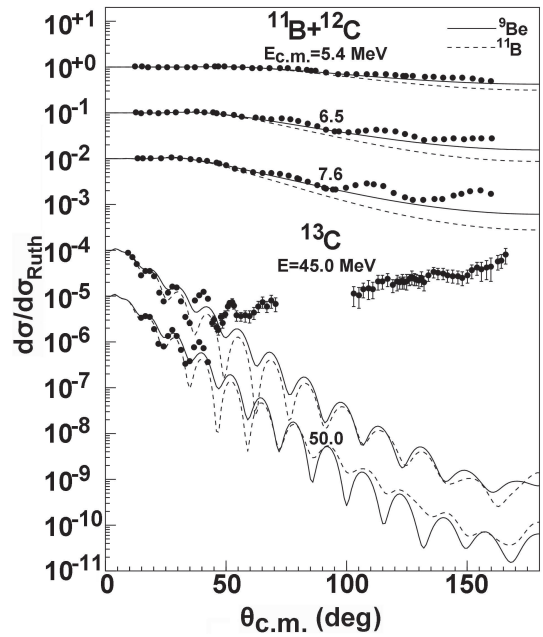


Fig. 19. Same as Fig. 14, but for $^{12,13}\text{C}$.

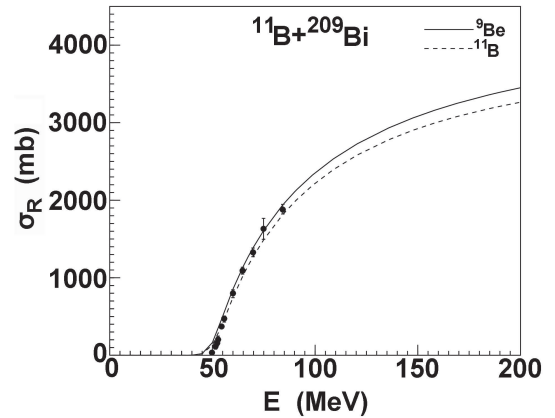


Fig. 20. Comparisons of ^{11}B total reaction cross-sections calculated using ^9Be and ^{11}B global OMPs with corresponding data for ^{209}Bi .

3 Summary

We predicted elastic scattering observables involving $^{8,10,11}\text{B}$ projectiles by applying the obtained global OMP of ^9Be . We compared these predictions with those of the other global OMPs, and investigated and analyzed them in detail. The theoretical results predicted using the global OMP of ^9Be give a more satisfactory description of the elastic scattering for $^{8,10,11}\text{B}$ projectiles for targets from ^{27}Al to ^{209}Bi . For the lighter targets, we made a tentative prediction. All of the results predicted using different global OMPs are not in good agreement with the experimental data in the backward-angle area for lighter targets. The reason is that the other reaction mechanisms have to be considered in the calculations for such light systems,

such as transfer or breakup. The present work shows that the global OMP of ^9Be is useful to systematically invest-

igate the reactions involving $^{8,10,11}\text{B}$ projectiles.

References

- 1 A. J. Koning and J. P. Delaroche, Nucl. Phys. A, **713**: 231 (2003)
- 2 L. R. Gasques, A. S. Freitas, and L. C. Chamon et al, Phys. Rev. C, **97**: 034629 (2018)
- 3 Yongli Xu, Yinlu Han, Jiaqi Hu et al, Phys. Rev. C, **97**: 014615 (2018)
- 4 Yongli Xu, Yinlu Han, Haiying Liang et al, Phys. Rev. C, **99**: 034618 (2019)
- 5 L. V. Grigorenko, B. V. Danilin, V. D. Efros et al, Phys. Rev. C, **57**: 2099(R) (1998)
- 6 V. Morcelle, R. Lichtentäler, A. Lépine-Szily et al, Phys. Rev. C, **95**: 014615 (2017)
- 7 J. J. Kolata, V. Guimarães, and E. F. Aguilera, Eur. Phys. J. A, **52**: 123 (2016)
- 8 E. F. Aguilera, E. Martinez-Quiroz, D. Lizcano et al, Phys. Rev. C, **79**: 021601(R) (2009)
- 9 M. Mazzocco, N. Keeley, A. Boiano et al, Phys. Rev. C, **100**: 024602 (2019)
- 10 Y. Y. Yang, J. S. Wang, Q. Wang et al, Phys. Rev. C, **87**: 044613 (2013)
- 11 Y. Y. Yang, X. Liu, D. Y. Pang et al, Phys. Rev. C, **98**: 044608 (2018)
- 12 A. Barioni, J. C. Zamora, V. Guimaraes et al, Phys. Rev. C, **84**: 014603 (2011)
- 13 G. Tabacaru, A. Azhari, J. Brinkley et al, Phys. Rev. C, **73**: 025808 (2006)
- 14 I. V. Kuznetsov, M. I. Ivanov, R. Kalpakchieva et al, IZV, **63**: 992 (1999)
- 15 C. Borcea, F. Carstoiu, F. Negoita et al, Nucl. Phys. A, **616**: 231 (1997)
- 16 Li Jiaxing, Xiao Guoqing, Guo Zhongyan et al, High Energy Physics and Nuclear Physics, **28**: 1256 (2004)
- 17 Xinwu Su, Yinlu Han, Haiying Liang, Zhendong Wu, Hairui Guo, and Chonghai Cai, Phys. Rev. C, **95**: 054606 (2017)
- 18 L. A. Parks, K. W. Kemper, R. I. Cutler et al, Phys. Rev. C, **19**: 2206 (1979)
- 19 V. Scarduelli, E. Crema, V. Guaráes et al, Phys. Rev. C, **96**: 054610 (2017)
- 20 M. A. G. Alvarez, M. Rodríguez-Gallardo, and L. R. Gasques et al, Phys. Rev. C, **98**: 024621 (2018)
- 21 C. W. Glover, K. W. Kemper, L. A. Parks et al, Nucl. Phys. A, **337**: 520 (1980)
- 22 T. Motobayashi, I. Kohno, T. Ooi et al, Nucl. Phys. A, **331**: 193 (1979)
- 23 Y. Y. Yang, J. S. Wang, Q. Wang et al, Phys. Rev. C, **90**: 014606 (2014)
- 24 K. Bodek, M. Hugi, J. Lang et al, Phys. Lett. B, **92**: 79 (1980)
- 25 A. M. Mukhamedzhanov, H. L. Clark, H. Dejbakhsh et al, Nucl. Phys. A, **631**: 788 (1998)
- 26 R. E. Warner, F. Carstoiu, J. A. Brown et al, Phys. Rev. C, **74**: 014605 (2006)
- 27 Jiaxing Li, Zhongyan Guo, Guoqing Xiao et al, High Energy Physics and Nuclear Physics, **26**: 683 (2002)
- 28 N. N. Deshmukh, V. Guimaraes, E. Crema et al, Phys. Rev. C, **92**: 054615 (2015)
- 29 A. Nurmela, P. Pusa, E. Rauhala et al, Nucl. Instrum. Methods B, **161**: 130 (2000)
- 30 P. K. Sahu, A. Saxena, R. K. Choudhury et al, Phys. Rev. C, **68**: 054612 (2003)
- 31 A. Shrivastava, S. Kailas, P. Singh et al, Nucl. Phys. A, **635**: 411 (1998)
- 32 L. Jarczyk, B. Kamys, A. Strzalsowski et al, Phys. Rev. C, **31**: 12 (1985)
- 33 S. Yu. Mezhevych, K. Rusek, A. T. Rudchik et al, Nucl. Phys. A, **724**: 29 (2003)
- 34 B. Guo, Z. H. Li, M. Lugaro et al, Astrophysical Journal, **756**: 193 (2012)